Journal of Theoretical Biology 255 (2008) 163–175

Contents lists available at ScienceDirect

Journal of Theoretical Biology

journal homepage: www.elsevier.com/locate/yjtbi

A hybrid agent-based approach for modeling microbiological systems

Zaiyi Guo [a], Peter M.A. Sloot [b], Joc Cing Tay [a,*]

[a] Evolutionary and Complex Systems Program, School of Computer Engineering, Nanyang Technological University, Blk N4 #2a-32 Nanyang Avenue, Singapore 639798, Singapore
[b] Section Computational Science, Universiteit van Amsterdam, Kruislaan 403, 1098 SJ Amsterdam, The Netherlands

ARTICLE INFO

Article history:
Received 17 December 2007
Received in revised form
13 June 2008
Accepted 5 August 2008
Available online 15 August 2008

Keywords:
Multi-layered simulation models
Chemotaxis
Under-agarose assay
Receptor kinetics

ABSTRACT

Models for systems biology commonly adopt Differential Equations or Agent-Based modeling approaches for simulating the processes as a whole. Models based on differential equations presuppose phenomenological intracellular behavioral mechanisms, while models based on Multi-Agent approach often use directly translated, and quantitatively less precise if-then logical rule constructs. We propose an extendible systems model based on a hybrid agent-based approach where biological cells are modeled as individuals (agents) while molecules are represented by quantities. This hybridization in entity representation entails a combined modeling strategy with agent-based behavioral rules and differential equations, thereby balancing the requirements of extendible model granularity with computational tractability. We demonstrate the efficacy of this approach with models of chemotaxis involving an assay of 10^3 cells and 1.2×10^6 molecules. The model produces cell migration patterns that are comparable to laboratory observations.

1. Introduction

A large part of *Systems Biology* (Kitano, 2002) involves the construction of mathematical and computational models that aid the understanding of how observed biological phenomena (such as the human immune response) emerge macroscopically through the integration of causal knowledge obtained from *in vitro* and *in vivo* experiments performed on *sub-parts* of the system. We will refer to them as *system models* in this paper. To simulate and analyze these *system-level* dynamics, such system models often sacrifice constituent details for computational tractability. For example, they may focus on intercellular (Celada and Seiden, 1992; Guo et al., 2005; Jacob et al., 2004; Nowak et al., 1991; Perelson and Nelson, 1999) rather than intracellular molecular interactions, such as the models for intracellular signal pathways and genetic regulatory networks (Ander et al., 2004; Emonet et al., 2005; Schaff et al., 1997; Takahashi et al., 2002).

As biological cell behaviors ultimately arise from intracellular molecular interactions, extending the model granularity to the *molecular level* becomes necessary in many cases, especially for continual integration of new research findings. For example, current drug treatments for HIV-1 through the use of reverse transcriptase and protease inhibitors are designed to block different stages of the reproduction process of HIV, which are processes taking place *within* the infected T helper cells (Fauci, 2003). Similarly, research on the conformational process of the gp120 surface protein on HIV virions help determine ways that inhibit their entry at target cell membranes (Stix, 2006). And ultimately, to be able to use agent-based models to verify various hypotheses of HIV pathogenesis on the human immune system (Guo et al., 2005), significant amount of microstructural details (e.g., gp120-induced cell syncytium and the filling of CD4 receptors) are required in order for the simulation results be useful for decision support (Gross and Strand, 2000).

Two common approaches for developing system models are Differential Equation (or DE, including ODE and PDE) models and Multi-Agent (or MA) models. DE models (Stekel et al., 1997) treat biological cells as populations (quantities), using an aggregate approach that disregards the cell's individual identity. Therefore, the ability to handle complex (possibly spatially explicit) heterogeneous cell behaviors that take place at the individual level is reduced. On the other hand, MA models (Celada and Seiden, 1992; Jacob et al., 2004) treat each cell as a unique individual (called *agent*) with distinct state variables and interaction history, thereby allowing possibly complex biological behaviors to be modeled for each cell type over a variety of environmental topologies. Typically, the cell behaviors in MA models are specified by a set of logical if-then rules. These two approaches have been contrasted in terms of assumptions, justifiability, realism, model granularity, implementation details, and computational tractability (Guo and Tay, 2005). MA models are believed to be more realistic (due to increased microstructural

* Corresponding author. Tel.: +65 6793 6528; fax: +65 6795 1615.
E-mail address: joccing@ieee.org (J.C. Tay).

0022-5193/$ - see front matter © 2008 Elsevier Ltd. All rights reserved.
doi:10.1016/j.jtbi.2008.08.008

complexity) but face issues of computation intractability and model scalability.

Though DE models and MA models are different modeling approaches, they are not necessarily mutually exclusive. In this paper we propose a *hybrid agent-based modeling approach* which treats chemical molecules as quantities and biological cells as individual agents. This is motivated by the morphological distinction between cells and molecules: where, compared to the former, molecules are much smaller (in the order of nanometers vs. cells in the order of micrometers), more abundant, have less complex behaviors and are well-characterized by physical laws. Though this modeling approach is agent-based in principle, DE techniques for characterizing macroscopic dynamics (such as reaction and diffusion equations) can be applied to molecular interactions on the cell surface and within the cells. We apply this proposed hybrid approach to model cell chemotaxis, a well-known phenomenon where cells are attracted to the source of certain chemical molecules (known as chemoattractant) by following the gradient. We choose this application for its illustrative value of modeling interactions between molecules and cells, a task that is difficult to achieve individually with DE or MA models. An accurate model of chemotaxis will give us increased confidence of modeling the higher level of biological processes that base on chemotactic movement of cells, such as lymphocytes migration in tissues during an immune response (Eisenbach et al., 2004). It has been demonstrated that MA models with accurately designed agent movement rules result in macroscopic behavioral patterns that better agree with observations (Hosseini, 2006; Railsback et al., 1999; Railsback and Harvey, 2002).

This paper is organized as follows. Section 2 describes the motivation for the hybrid treatment of cells as individuals and molecules as quantities within a single MA model. Section 3 describes the hybrid agent-based design approach, which consists of developing (1) an environment model for interactions between quantity-based molecules and individual-based biological cells (agents) and (2) specifying general and extendible agent behaviors. Section 4 presents the application of the hybrid modeling approach to the chemotaxis phenomenon with an *in silico* Under-Agarose Assay and cell–molecule interactions involving receptor kinetics. Section 5 concludes the paper.

2. Motivation

Cells and molecules are basic building blocks in all biological systems. Any nontrivial system-level modeling attempt (such as to determine the efficacy of drug treatments for HIV-1 infections within a virtualized laboratory (Sloot et al., 2006)) invariably needs to deal with interactions of the two. Taking the human immune system as an example, the major cellular players are leucocytes, including phagocytes (mononuclear phagocytes, neutrophils, eosinophils), auxiliary cells (basophils, mast cells, platelets), and lymphocytes (T cells, B cells, large granular lymphocytes) (Janeway et al., 2001; Roitt and Delves, 2001). The intercellular interactions take place through direct cell contact and chemokine passing. Chemokines are molecules that are secreted by one type of cell and received by another type of cell. These molecules affect by binding to the receptor molecules expressed on the target cells, starting a chain of molecular reactions within the cell which leads to a state change of the cell, such as activation or migration. For example, Th2 cells (a subset of T helper cells) release cytokines such as interleukins IL-4 and -5, which are required for B cell differentiation. In general, cells interact in a deliberate and systematic way through direct contact or through the exchange of information via chemokine secretion.

Naively, DE models for biological cell populations commonly assume that collectively, cell interactions obey a mass action law and the diffusion law for their movements. The former means the likelihood that two cells will interact is proportional to the concentration of each of the two types of cells, while the latter implies that biological cells move randomly, like molecules. However, the basic form of the reaction–diffusion equations are not readily applicable to many biological phenomena, where the cellular encounter is in reality, known to be more systematic rather than random. As an example, cell distributions within a lymph node are non-even: B cells and T cells concentrate in different areas known as B zones and T zones (Janeway et al., 2001). Research has revealed that T cells are recruited to the T zone through the interaction between T cell's CCR7 receptor and its ligands, SLC and ELC (Cyster, 2000; Weninger et al., 2001), though it has not been firmly established whether the movements entirely attributed to chemotaxis (Wei et al., 2003). Similarly, dendritic cells, which present antigens to T cells so as to trigger an immune response, also bear CCR7 on their surface and are attracted to the same T zone (Cyster, 1999; Sallusto et al., 1998; Sozzani et al., 1998). As a result, the chance of interaction between dendritic cells and T cells (and hence the chance that T cells recognize antigens) are significantly increased as compared to the simplistic assumption that they interact only through Brownian cell movements. It is generally difficult for DE models to handle the multiple roles that a biological cell may undertake in its lifetime (especially for immune cells).

The need to use an individual-based approach for modeling biological cells arises from their wide range of possible states and nonlinearly interacting behaviors (Guo and Tay, 2005). In some MA models (Guo et al., 2005; Kleinstein and Seiden, 2000), molecules (e.g., antibodies) are also modeled as individuals. We believe, however, that molecules and cells are sufficiently different to warrant the combined use of distinct but complementary modeling strategies for each type of entity. The primary reasons for distinguishing between them (for modeling purposes) are:

(1) *Relative scales*: The size of molecules (in the order of nanometers) are several orders of magnitude smaller than cells (in the order of micrometers) (Nelson, 2004). The so-called molecule–cell interaction is ultimately a molecule–molecule interaction: some ligand molecules in the environment interact with certain receptor molecules on the cell surface.
(2) *Relative population sizes*: The quantities of molecules are potentially much larger than the quantity of cells. For example, it is estimated that every plasma cell may produce antibody molecules at a rate of $2000\,s^{-1}$ (Merieb, 2006). Modeling molecules as individuals would therefore be computationally intractable.
(3) *Relative complexity*: The behaviors of molecules are much simpler than those of cells. Individually, molecular interactions can be considered as chemical reactions, and collectively, the resulting dynamics are quantitatively captured by the law of mass action. Their random movement at the individual level is also captured by Fick's law of diffusion at the population level. Using mass action law and the diffusion law eliminates the need to model molecules individually. On the other hand, cells are much more complex and it is difficult to describe their aggregate behaviors using mathematical formulas without considerable simplification (which is the main issue with DE models).

The above differences between molecules and cells motivate our hybrid approach towards the modeling of biological cells as individuals and molecules as quantities. In the next section, we describe this approach in detail.

3. A hybrid modeling approach for extended system models

To model a microbiological system of cells and molecules, we consider model hybridization at two levels: globally in the *environment*, and locally with a *cell* (on its surface and within its body).

3.1. Environment modeling

The *environment* is where biological cells and molecules reside and interact. The environment model handles the storage and provision of spatial proximity information of cells and molecules. It also handles environment level events that are exogenous to individual agents, such as the spread of inflammatory signals, blood flows, and lymphoid fluid flows. We view the environment not merely as a passive 'holder' to place the agents, but as an active entity with its own activities and special properties (e.g., blood flows) which can greatly influence the behaviors of the agents (Weyns et al., 2006).

Our model of the environment consists of three functional layers superimposed in the same space:

(1) An *Agent Holder Layer*, where all agents (cells) reside.
(2) A *Molecule Space Layer*, where all molecular distributions are recorded.
(3) A *Flow Field Layer*, where background flows, such as blood flows and lymph flows are modeled.

Each point in the environmental space is a composition of all the layer functionalities at that particular coordinate. To illustrate, Fig. 1 shows the environmental space as three layers of two-dimensional (2-D) planes, but the concepts are not necessarily restricted to a 2-D space but applicable to any number of dimensions. The layers are classified into *continuous* and *discrete space* layers. In continuous space layers, real values can be specified for the coordinates but in the discrete space layers, values are defined only at discrete 'grid points'. When composing discrete and continuous layers, values at intermediate coordinates are determined using interpolation. Of the three layers, only the *Agent Holder Layer* uses a continuous space. We next describe each layer in detail.

The *Agent Holder Layer* contains all the *agents*. The *agents* denote entities that are modeled at the *individual* level, and here we mainly refer to biological cells. The location of each agent is specified by its real coordinates in this layer. In the simplest case where the agents are modeled as spheres, two agents collide if the distance between their coordinates is shorter than the sum of their radius. This physical contact may result in more inter-agent interactions (defined by agent behavioral rules).

The *Molecule Space Layer* and the *Flow Field Layer* share a common mesh grid structure, which is a discretized version of the space. We use ΔL to denote the distance between two neighboring mesh grid points. The value of ΔL determines the *granularity* of the discrete space. A grid point indexed by (i, j) corresponds to a real-valued coordinate $(i\,\Delta L, j\,\Delta L)$ in the continuous space of the Agent Holder Layer. Therefore, each agent is necessarily located within some grid cell. This correspondence in spatial locations is the basis of the 'communication' between layers.

The *Molecule Space Layer* consists of multiple sub-layers, each representing the spatial distribution of a certain type of molecule. The local molecular quantity (number of molecules) at each grid point (i, j) is denoted by $Q_{i,j}$. The change in the spatial distribution of molecules is subject to the following simultaneously occurring events:

(1) *Production*: Cells may synthesize and release cytokines into its neighborhood.
(2) *Diffusion*: The molecules spread due to Brownian movement.
(3) *External flow*: For example, in the blood vessels and lymph duct, the molecules are 'pushed' by the local fluid flow.
(4) *Consumption/degradation*: Certain molecules are 'consumed' by binding to cell receptors. Molecules also decay through various pathways (e.g., instability, enzymic reactions).

The net change of $Q_{i,j}$ over time Δt is the combined result of the factors above:

$$\frac{\Delta Q_{i,j}}{\Delta t} = \left.\frac{\Delta Q_{i,j}}{\Delta t}\right|_{production} + \left.\frac{\Delta Q_{i,j}}{\Delta t}\right|_{consumption} + \left.\frac{\Delta Q_{i,j}}{\Delta t}\right|_{diffusion} + \left.\frac{\Delta Q_{i,j}}{\Delta t}\right|_{decay} + \left.\frac{\Delta Q_{i,j}}{\Delta t}\right|_{flow} \quad (1)$$

As we are using agents to model individual cells, the first two terms emerge from the collective interactions of cells and molecules. Therefore, these two terms do not have explicit mathematical expressions. The change of $Q_{i,j}$ due to *random movement* is modeled using the diffusion law. After applying the finite difference method to the diffusion law over a 2-D space, we obtain

$$\left.\frac{\Delta Q_{i,j}}{\Delta t}\right|_{diffusion} = \frac{D}{\Delta L^2}(Q_{i-1,j} + Q_{i+1,j} + Q_{i,j-1} + Q_{i,j+1} - 4Q_{i,j}) \quad (2)$$

where ΔL is the distance between two neighboring grid points and D is the diffusion constant. For this numerical solution to be stable, it requires $\Delta t \leqslant \Delta L^2/4D$ (Heath, 2005). Intuitively, Eq. (2) says that $\Delta Q_{i,j}/\Delta t|_{diffusion}$, the change of the molecular quantity at

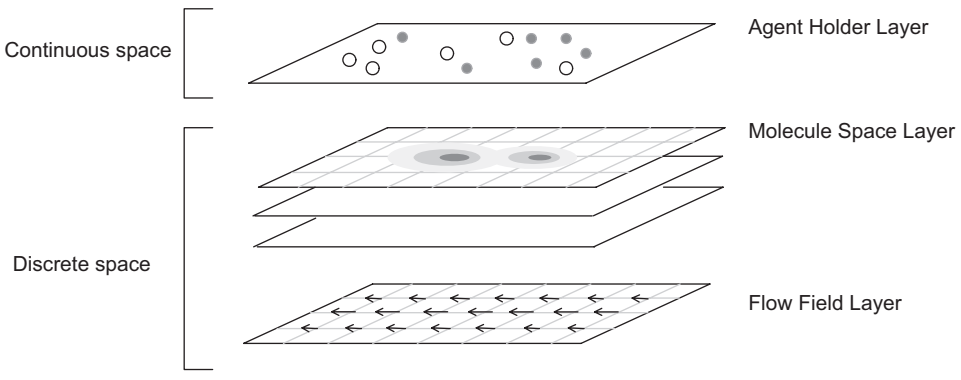

Fig. 1. Three-layer structure of the simulated environment.

(i, j) over a time step of Δt due to diffusion is the net summation of the outflows and inflows at (i, j) from the neighboring grid points.

The number of molecules that are removed due to decay within time-step Δt is approximated by

$$\left.\frac{\Delta Q_{i,j}}{\Delta t}\right|_{decay} = -\lambda Q_{i,j} \tag{3}$$

where λ is the decay constant.

The *Flow Field Layer* characterizes the background flow in the environment. It represents the systematic transport superimposed onto the random movements (by diffusion) of molecules and agents. At each grid point (i, j), the flow velocity is given by $\mathbf{F}_{i,j}$. A simple example is laminar flow, which is the normal condition for blood flow in most of the blood vessels: the flow velocity is the highest in the center of the vessel and lowest along the vessel wall (Klabunde, 2006). Turbulent flows occur when laminar flow is disturbed, such as at the branch point of the vessels (Klabunde, 2006). These flow profiles are environment-dependent and are to be modeled by the Flow Field Layer.

The flows specified by the Flow Field Layer influence the spatial distribution of the molecules (in the Molecule Space Layer) by shifting the distribution towards the direction of flow. Consider a grid point indexed at (i, j) in Fig. 2 has the real coordinate is $(i\,\Delta L, j\,\Delta L)$. Its governing space, $\mathbf{V}_{i,j}$ is the rectangle $(\Delta L \times \Delta L)$ centered at $(i\,\Delta L, j\,\Delta L)$. Let $Q_{i,j}$ denote the molecular quantity within $\mathbf{V}_{i,j}$, and let $\mathbf{F}_{i,j}(=(\mathbf{F}_{i,j,x}, \mathbf{F}_{i,j,y}))$ denote the flow velocity (vector) at $(i\Delta L, j\Delta L)$. Within Δt, the quantity $Q_{i,j}$ is shifted along the direction of $\mathbf{F}_{i,j}$ by $(F_{i,j,x}\,\Delta t, F_{i,j,y}\,\Delta t)$. Let $\mathbf{V}'_{i,j}$ be an imaginary rectangle space $(\Delta L \times \Delta L)$ centered at $(i\,\Delta L + F_{i,j,x}\,\Delta t, j\,\Delta L + F_{i,j,y}\,\Delta t)$, that is, the "shifted" space that contains $Q_{i,j}$ after Δt. Let $S_{u,v\to i,j}$ denote the overlapping space between $\mathbf{V}_{i,j}$ and $\mathbf{V}'_{u,v}$ (i.e., the governing space of grid point indexed at (u, v) shifted by its local flow $\mathbf{F}_{u,v}$). Hence the proportion of $Q_{i,j}$ that remains in $\mathbf{V}_{i,j}$ is $Q_{i,j}S_{i,j\to i,j}/\Delta L^2$, and the rest are distributed to the governing space of the neighboring grid points. The molecular quantity within $\mathbf{V}_{i,j}$ after Δt is the sum of the "shifted" quantities (due to flow) from all the neighboring grid points that fall into $\mathbf{V}_{i,j}$. Therefore, the change of molecular quantity at (i, j) due to flow is

$$\Delta Q_{i,j}|_{flow} = \sum_{u=i-1}^{u=i+1}\sum_{v=j-1}^{v=j+1} Q_{i,j}S_{u,v\to i,j}/\Delta L^2 - Q_{i,j} \tag{4}$$

The position of agents in the Agent Holder Layer is affected by both the Molecule Space Layer and the Flow Field Layer. A biological cell is passively driven by the background flows (e.g., the blood flow). It also moves not only passively, but also actively in response to the local molecular concentration and gradient, exhibiting *chemokinesis* and *chemotaxis*. Formally, we model the displacement $\Delta\mathbf{p}$ of an agent in time Δt as a function of the local flow velocity $\mathbf{F}_\mathbf{p}$, the local molecular concentrations $C_{\mathbf{m},\mathbf{p}}$ and gradients $\mathbf{G}_{\mathbf{m},\mathbf{p}}$ for a set of molecules $\mathbf{m}$ (Eq. (5)). The definition of $\mathbf{d}(\cdot)$, that is, how an agent combines the effect of the external field, chemokinesis and chemotaxis is determined by the agent rule set, which is in turn an experimentally observable and verifiable set of biological functions pertaining to some type of cell. Some types of agents may be highly motile while others are structural in function, hence immovable. The agent may be observed to respond to only specific types of $\mathbf{m}$, depending on its type and state. Whether $\mathbf{d}(\cdot)$ is expressed as mathematical equations or if-then decision logics or a hybrid of both is generally subject to the modeler's knowledge or experience:

$$\Delta\mathbf{p}/\Delta t = \mathbf{d}(\mathbf{F}_\mathbf{p}, C_{\mathbf{m},\mathbf{p}}, \mathbf{G}_{\mathbf{m},\mathbf{p}}) \tag{5}$$

In our model, the environment provides agents with discrete information on local concentrations and gradients of molecule types as well as the local flow vector. Determining the local effect of this information for an Agent's position (within the Agent Holder Layer) requires interpolations from quantities defined at neighboring grid points. We adopt the bilinear interpolation (for a 2D space) for its simplicity and efficiency as it requires considerably fewer points than the cubic or spline method (4 vs. 16 in 2-D space). Consider the agent in Fig. 3 (depicted by a circle), whose nearest grid points are indexed by (i, j), $(i, j{+}1)$, $(i{+}1, j)$, and $(i{+}1, j{+}1)$, respectively. The local concentrationof molecule m at the agent's position obtained through bilinear interpolation is

$$\begin{aligned} C_{m,\mathbf{p}} = \Delta L^{-4}(&Q_{i,j}(\Delta L - \Delta x)(\Delta L - \Delta y) + Q_{i+1,j}\Delta x(\Delta L - \Delta y) \\ &+ Q_{i,j+1}(\Delta L - \Delta x)\Delta y + Q_{i+1,j+1}\Delta x\Delta y) \end{aligned} \tag{6}$$

The local flow velocity is

$$\begin{aligned} \mathbf{F}_\mathbf{p} = &\mathbf{F}_{i,j}(\Delta L - \Delta x)(\Delta L - \Delta y)/\Delta L^2 + \mathbf{F}_{i+1,j}\Delta x(\Delta L - \Delta y)/\Delta L^2 \\ &+ \mathbf{F}_{i,j+1}(\Delta L - \Delta x)\Delta y/\Delta L^2 + \mathbf{F}_{i+1,j+1}\Delta x\Delta y/\Delta L^2 \end{aligned} \tag{7}$$

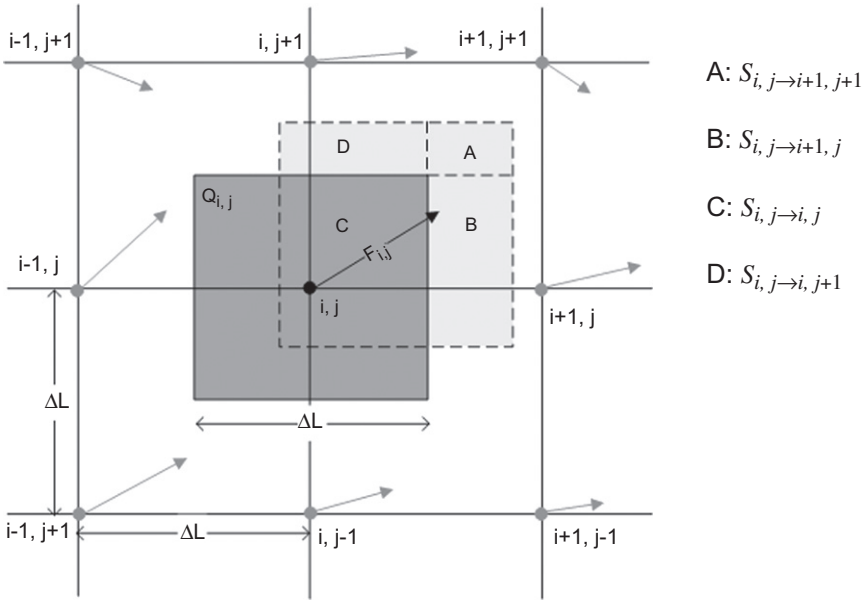

Fig. 2. Modeling the effect of flow on molecular distribution.

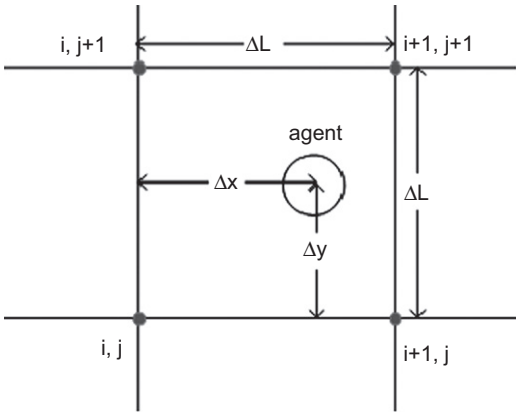

Fig. 3. Sampling of the local molecular concentration and gradient by an agent (cell).

The local gradient $\mathbf{G}_{m,\mathbf{p}} = \nabla C_{m,\mathbf{p}}$ is a vector with components:

$$G_x = \Delta L^{-4}((Q_{i+1,j} - Q_{i,j})(\Delta L - \Delta y) + (Q_{i+1,j+1} - Q_{i,j+1})\Delta y)$$
$$G_y = \Delta L^{-4}((Q_{i,j+1} - Q_{i,j})(\Delta L - \Delta x) + (Q_{i+1,j+1} - Q_{i+1,j})\Delta x) \quad (8)$$

We have described a hybrid model of the virtual environment and the general interactions between agents (individual biological cells) and molecules (quantities) in such an environment. Though they reside in layers with different spatial granularities (discrete or continuous), we have shown how interactions among layers can be predicted through simple interpolation. We next introduce the behavioral rule building scheme for the biological cells.

3.2. Behavioral modeling for agents

As described in Sections 2 and 3.1, biological cells are modeled at the individual level as *agents*. Agent behavior models (for biological cells) can be constructed with several levels of granularities. They can include specific details on the (known) intracellular dynamics of molecular signaling pathways and genetic networks (Ander et al., 2004; Emonet et al., 2005; Schaff et al., 1997; Takahashi et al., 2002), or abstract a number of if-then rules (Grilo et al., 1999; Guo et al., 2005; Jacob et al., 2004) and treat intracellular activities as "black boxes". A complete bottom-up approach (i.e., from molecular level or even atomic level to the system level) is generally considered infeasible due to its high computational cost (Takahashi et al., 2005). The common practice is in line with the principle of Occam's razor: only concepts that are necessary for explanation are to be modeled. Therefore, the justification of increasing the model granularity needs to be based on identifying the limitations of the current models.

We examine a simple model for B cell's behavior in collision with a virus (Jacob et al., 2004):

```
IF collision with virus & active:
   Increment virus-collision counter.
   IF virus-collision counter >threshold:
      IF enough helper T cells:
         Secrete antibodies.
         Create new B cell.
```

The rule simplifies the process of collision and of virus recognition, both of which, in reality depends on the probabilistic success of molecule-to-receptor chemical bindings, but these molecular details are omitted in the above example. It suffices to replace the molecular details with a set of higher-level if-then statements, because (1) under normal and healthy human conditions, the aggregate outcome of these interactions are usually predictable and directly measurable and (2) the purpose of the model is more for reproducing the qualitative patterns than for making quantitative predictions.

Such phenomenological abstractions become a limitation when the purpose of the application is to compare explanations and verify hypotheses. For models that are developed for infectious diseases, such as HIV-1, where the normal response of the immune cells are interrupted and become less predictable due to molecular level interactions between the virus and the cell, such a simplification becomes insufficient. Several pathogenic mechanisms have been experimentally verified to exist, which motivates the construction of hypothesis verification models for quantifying which mechanism is more statistically significant (Guo et al., 2005). For this purpose, it is vital to model the different hypothetical situations based on a common denominator, which is usually at the molecular level (based on literature survey). For models that are more *explorative* than *illustrative*, the incorporation of cell–molecule interactions into agent rules becomes necessary in order to achieve necessary quantitative accuracy.

On the other hand, computational tractability mandates that the model be simple and avoid unnecessary details. The appropriate balance between the orthogonal dimensions of model efficiency and granularity varies for each application and must be carefully chosen with the expert's domain knowledge against that of the model's intended purpose. While much of scientific modeling remains an art, we do expect that an agent's behavior model be "non-uniform" in that it needs to handle events at different scales, such as

- Different types of cells are modeled at different granularity levels: some incorporate selective signaling pathways, while others are as simple as "black boxes". This can be achieved by applying suitable techniques (e.g., if-then rules or differential equations) for different parts of the model.
- Events are taking place at different timescales: molecular interactions occur at a smaller scale than compared to cellular level events. This can be achieved by an event-scheduling-based update scheme (Guo and Tay, 2007) which avoids the use of a uniform update frequency throughout the model.

We next describe a simple example of a receptor kinetics model for a biological cell that uses differential equations for updating the agent's internal status. The model is more detailed than a "black box" as in many MA models, but is still far less detailed than that of whole-cell models (Ander et al., 2004; Emonet et al., 2005; Schaff et al., 1997; Takahashi et al., 2002). This simple receptor kinetics model will be subsequently used for the chemotaxis experiment to be described in Section 4.

3.2.1. Model for cell receptor kinetics

We consider three interdependent molecular events for receptor kinetics (Zigmond et al., 1982):

(1) *Receptor–ligand binding*, where free ligand molecules bind to receptors on the cell surface.
(2) *Receptor internalization and ligand consumption*, where the receptor–ligand complex is internalized into the cytosol, and the ligand is 'used up' or digested by other biological processes.
(3) *Receptor recycling*, where the previously internalized receptors are returned to the cell surface, to be made available for binding again.

Though our hybrid approach treats molecular interactions macroscopically as quantities, it is instructive to understand how the collective effects of these interactions give rise to the macroscopic descriptions. Readers who frequently use a mathematical modeling approach would find the following equations familiar. However, we need to emphasize that instead of a global description of the molecular kinetics, these equations are part of the agent behavioral rules, that is, at the scale of individual agents.

Consider a microscopic event where an individual ligand L meets an individual receptor R and binds to it, producing an 'occupied receptor' LR. This event can be described as a chemical equation of the form:

$$L + R \xrightarrow{k_b} LR \quad \text{(receptor}-\text{ligand binding)} \tag{9}$$

The left-hand side of Eq. (9) indicates that for a single binding event, one L and one R are consumed, and the right-hand side indicates the result that one LR is produced. Microscopically, the parameter k_b is a quantitative indication of how likely the binding would happen given that the two reactant molecules meet. Macroscopically, each binding event reduces the R and L quantities (by Eq. (1)) and increases the LR quantity (by Eq. (1)). The rate at which the binding process takes place is proportional to k_b and the quantities (or concentrations) of R and L. Based on the mass action law, it is straightforward to derive the corresponding macroscopic description of Eq. (9) as differential equations:

$$\left.\frac{\mathrm{d}[L]}{\mathrm{d}t}\right|_b = \left.\frac{\mathrm{d}[R]}{\mathrm{d}t}\right|_b = -\left.\frac{\mathrm{d}[LR]}{\mathrm{d}t}\right|_b = -K_b[L][R] \tag{10}$$

Traditionally, the notation $[\cdot]$ denotes the *concentration* of molecules in the whole space (having units M or mole L^{-1}), but here we redefine it as the *quantity* of molecules *in the proximity of*, or *within* the agent. That is, $[L]$ is the *local* number of ligand molecules 'available' to the agent while $[R]$ is the number of receptors expressed on the agent (cell) surface. The rate constant K_b is proportional to its microscopic counterpart k_b and denotes the number of bindings per unit time per pair of reactants. One would recognize K_b to be similar to the *forward rate constant* or *association rate constant* in enzyme kinetics (Mathews et al., 2000), except for the difference in the unit. Enzyme kinetics typically deals with concentrations (assumed uniform distribution in space) while here we deal with quantities that are local to each agent. For simplicity, we assume that the disassociation of R and L is rare and can be ignored. The equations in Eq. (10) describe the change in molecular quantity local to a single agent, therefore they can be considered as agent rules expressed in equational form.

We next consider the events of receptor internalization/ligand consumption and receptor recycling. One example of these processes is receptor-mediated endocytosis (Guyton and Hall, 2000), where a biological cell takes in molecules that are too big to enter the cell through diffusion or transport proteins. The bound ligand is disassociated from the receptor and 'consumed' by other biological processes. The freed receptor is then returned to the cell surface. The microscopic chemical equations are:

$$LR \xrightarrow{k_i} R^* \quad \text{(receptor internalization and ligand consumption)} \tag{11}$$

$$R^* \xrightarrow{k_r} R \quad \text{(receptor recycling)} \tag{12}$$

where k_i is the rate at which a single LR molecule converts to a R^*, a free receptor molecule still in the cytosol, and k_r is the rate at which the receptor is returned to the surface. The corresponding macroscopic (local to the particular agent's environment) differential equations are:

$$\left.\frac{\mathrm{d}[LR]}{\mathrm{d}t}\right|_i = -\left.\frac{\mathrm{d}[R^*]}{\mathrm{d}t}\right|_i = -K_i[LR] \tag{13}$$

$$\left.\frac{\mathrm{d}[R^*]}{\mathrm{d}t}\right|_r = -\left.\frac{\mathrm{d}[R]}{\mathrm{d}t}\right|_r = -K_r[R^*] \tag{14}$$

The effect of macroscopic Eqs. (10), (13), (14) are expressed by an agent's behavioral rule (shown in Table 1). Since the molecular events are taking place concurrently, we must avoid a predefined order of performing these updates; that is, they should be executed *in parallel*. One way is to randomize the order of their execution. Alternatively, we can achieve true parallelism by combining Eqs. (10), (13), and (14) so that the factors affecting the molecular quantity $[X]$ are arranged to appear on the right-hand side of the same equation. The rearrangement is mathematically expressed as follows:

$$\frac{\mathrm{d}[X]}{\mathrm{d}t} = \sum_s \left.\frac{\mathrm{d}[X]}{\mathrm{d}t}\right|_s, \quad \text{where } s \in \{b, i, r\},\ X \in \{R, L, LR, R^*\} \tag{15}$$

This gives rise to the system of coupled equations shown in the right-hand column of Table 2. The revised version of the agent rule from Table 2 is given in Table 3. These equations are used in the action part of the agent rule to update the local molecule quantities $[L]$, $[R]$, $[LR]$, and $[R^*]$. As the ligand quantity $[L]$ varies with the agent's location, it adds nondeterministic factors to the results, even the rules are expressed in terms of deterministic equations.

The rule we specify here is quite flat as there is only one proposition and all the equations appear in the action part. However, it is possible to specify more complex situations that an agent can be in, and the different responses it could make.

Table 1
Agent rule: receptor–ligand interaction

```
If Alive Then
   Sample the environment: getcurrent local ligand quantity [L]:
   Get the values of individually stored quantities [R], [LR], and
   [R*]
   Perform followingupdating rules in parallel:
   (a) reduce [L], [R]by Kb[L][R] Δt, and increase [LR]by
   Kb[L][R] Δt(receptor-ligand binding)
   (b) reduce [LR]by Ki[LR] Δt, and increase [R*]by Ki[LR] Δt(receptor
   internalization and ligand consumption)
   (c) reduce [R*]by Kr[R*] Δt, and increase [R]by Kr[R*] Δt(receptor
   recycling)

End If
```

Table 2
Microscopic rules and macroscopic equations for receptor–ligand interactions that are local to an agent's environment

Individual reactions	Quantity changes (combined updating rule)
Receptor–ligand binding	
$L + R \xrightarrow{k_b} LR$	$\frac{\mathrm{d}[L]}{\mathrm{d}t} = -K_b[L][R]$ $\frac{\mathrm{d}[R]}{\mathrm{d}t} = -K_b[L][R] + K_r[R^*]$
Receptor internalization and ligand consumption	
$LR \xrightarrow{k_i} R^*$	$\frac{\mathrm{d}[LR]}{\mathrm{d}t} = K_b[L][R] - K_i[LR]$
Receptor recycling	
$R^* \xrightarrow{k_r} R$	$\frac{\mathrm{d}[R^*]}{\mathrm{d}t} = K_i[LR] - K_r[R^*]$

Table 3
Agent rule: receptor–ligand interaction (rewritten for parallel updating)

```
If Alive Then
   Sample the environment: get current local Ligand quantity[L]:
   Get the values of individually stored quantities [R], [LR], and
   [R*]
   Compute d[L], d[R], d[LR], d[R*] using equations in Table 2
   Update local quantities: [X] = [X]+d[X] (X∈{R, L, LR, R*})

End If
```

3.3. Summary

We have proposed an agent-based hybrid modeling approach and its implementation at both the environment and agent levels. Hybridization here refers to the differentiated treatment of biological cells and chemical molecules, with the former modeled as individual agents and the latter as quantities (Section 2 has provided the motivations). The accomplishment of this objective requires three tasks. Firstly, we have shown how the proposed approach combines the use of quantity-based differential equations and individual-based if-then rules. Differential equations are applied to update the environmental level molecular distributions, and can also be nested in the agent's if-then rules to update the intracellular molecule levels. Secondly, in order to represent the individuals and quantities at the same time in the environment, we have shown how the space is modeled both continuously and discretely through functional layering. Individuals in the continuous space learn about the local environment by interpolating the molecular quantities stored in the grid points of the discrete space. Thirdly, when cells are treated as individuals, its internal properties (state variables and updating rules) can be considered as a black-box or be explicitly modeled as a network of rules and states that represent the molecular interactions. To further enunciate the pattern of receptor–ligand interactions to the level of intracellular molecular interactions, we have shown how quantity-based differential equations can be nested within individual agent rules.

In the next section we model the phenomenon of chemotaxis as an example of our proposed agent-based hybrid modeling approach.

4. Case study: modeling chemotaxis

Chemotaxis refers to the directed cell movement towards or away from a chemical source (chemoattractant or chemorepellent) by sensing and following the *chemical gradient* (Eisenbach et al., 2004) in its immediate neighborhood. Through chemotaxis, a sperm cell finds the ovum, a white blood cell finds the place of injury or inflammation, and a nerve cell grows its axon to establish synaptic connections (Eisenbach et al., 2004). Chemotaxis relates the movement patterns of cells to the spatial distribution of molecules, hence they serve as a good benchmark for illustrating the hybrid modeling scheme proposed in Section 3.

The phenomena of chemotaxis has been investigated as well as modeled extensively. The most popular mathematical model is the Keller-Segel model (Keller and Segel, 1971a, b; Sherratt, 1994), which is a PDE model which describes cells and molecules as population level quantities. The model is *phenomenological* in that it abstracts away molecular details of the transduction of extracellular signals to cell locomotion as the detailed molecular interactions were not well-understood at that time. In the past decade however, much of bioscience research has been devoted to discovering the mechanisms that transduce the extracellular chemical signals into cell locomotion (Firtel and Chung, 2000; Jones, 2000; Lin et al., 2004; Mitchison and Cramer, 1996; Parent and Devreotes, 1999; Sanchez-Madrid and Del Pozo, 1999). These include molecular events such as G-protein activation, lipid remodeling, protein kinase activation, calcium elevation (Eisenbach et al., 2004; Firtel and Chung, 2000), and cellular events such as cell polarization, pseudopod extension, excitation and adaptation (Eisenbach et al., 2004; Sanchez-Madrid and Del Pozo, 1999). Therefore, it can be expected that newer chemotaxis models need to incorporate intracellular mechanisms in order to model the newer findings at the intracellular level. Our model presented here is a preliminary version of such an attempt. The simple receptor kinetics presented in Section 3.2 are incorporated as the intracellular mechanisms of the chemotaxis model.

4.1. Agent rules for movement

The chemotaxis model consists of a hypothetical motile cell (or M cell) population and the chemoattractant molecules L (ligand). The M cell is capable of both random movement as well as directed movement towards L. We describe the total displacement $\Delta\mathbf{p}$ over an arbitrary update interval Δt, as a linear summation of the random displacement $\Delta\mathbf{p}_{random}$, displacement due to local flow $\Delta\mathbf{p}_{flow}$, and the chemotactic displacement $\Delta\mathbf{p}_{chemo}$ that take place over Δt:

$$\Delta\mathbf{p} = \Delta\mathbf{p}_{random} + \Delta\mathbf{p}_{flow} + \Delta\mathbf{p}_{chemo} \tag{16}$$

Eq. (16) is an instantiation of Eq. (5). $\Delta\mathbf{p}_{random}$ has an arbitrary direction (random movement). Its magnitude is the product of the update interval Δt and the random movement speed (a random value between 0 and l). $\Delta\mathbf{p}_{flow}$ is the product of the local flow velocity $\mathbf{F_p}$ and time duration Δt. $\Delta\mathbf{p}_{chemo}$ converts local ligand concentration $C_{\mathbf{m,p}}$ and gradient information $\mathbf{G}_{\mathbf{m,p}}$ into a vector, which will be defined later in this section.

For a particular M cell, the update interval Δt is the period of time between two consecutive calls to its *move* method. We adopt an event-scheduling-based update scheme (Guo and Tay, 2007) that simulates all the biological processes as a series of discrete events, which allows arbitrary lengths of time between events. For efficiency reasons, the discrete event scheduler allows us to incorporate a simple "negative feedback loop" between the update interval Δt and the cell's movement speed. Specifically, we assume the following relationship:

$$\Delta t_{n+1} = 5\exp(-\Delta\mathbf{p}/\Delta t_n) + 1 \tag{17}$$

That is, the slower the current movement speed ($\Delta\mathbf{p}/\Delta t_n$), the less likely that the cell will experience rapid movement in the near future, hence the next update interval Δt_{n+1} can be set longer to reduce the computational cost. The update interval therefore ranges from 1 (the update interval of molecular diffusions) to 6 (unit: minute) based on Eq. (17). Experiments have shown that such an implementation does not alter the simulation results in terms of aggregate cell movement behaviors.

For the chemotactic displacement $\Delta\mathbf{p}_{chemo}$, we adopt the quantitative hypothesis that chemotactic response is proportional to the receptor difference in receptor occupancy of the front and the rear of the cell (Devreotes and Zigmond, 1988). The equations for receptor–ligand binding, receptor internalization and receptor recycling are described in Section 3.2 (Eqs. in Table 2). Here we extend its formulation to determine the effect on chemotactic movement. Let r and V represent the radius and the volume of an M cell, and let $[R]$, $[LR]$, $[R^*]$ represent the quantity of the free surface receptors, occupied surface receptors, and the internalized receptors, respectively. The amount of ligand available at the front

and the rear of the cell is approximated by

$$[L]_{front} = (C + |\mathbf{G}|r)V/2 \tag{18}$$

$$[L]_{rear} = (C - |\mathbf{G}|r)V/2 \tag{19}$$

The number of newly bound receptors (LR) for the period Δt at the front and rear of the cell are:

$$\Delta[LR]_{front} = K_b[L]_{front}[R]_{front}\,\Delta t \tag{20}$$

$$\Delta[LR]_{rear} = K_b[L]_{rear}[R]_{rear}\,\Delta t \tag{21}$$

where $[R]_{front} = [R]_{rear} = [R]/2$ by assuming the free receptors are equally distributed on the cell surface. Recall from Eq. (10) that K_b is the binding rate of the ligand and the receptor.

From Eqs. (20) and (21), the difference in newly bounded receptors in Δt is therefore

$$\Delta[LR]_{diff} = K_b([L]_{front} - [L]_{rear})[R]\,\Delta t/2 \tag{22}$$

Assuming linear dependency of the chemotactic displacement on the difference in newly bounded receptors gives rise to

$$\frac{\Delta \mathbf{p}_{chemo}}{\Delta t} = k(\Delta[LR]_{diff}/\Delta t)(\mathbf{G}/|\mathbf{G}|) \tag{23}$$

where k is a proportional parameter. The larger the value of k, the more responsive the cell movement is to the occupancy difference in newly bounded receptors at its front and its rear.

4.2. Experimental design

We conduct an *in silico* experiment to simulate the Under-Agarose Assay, which was designed to investigate the *in vitro* chemotactic behavior of leucocytes (e.g., neutrophils, macrophages, and monocytes) (Heit and Kubes, 2003; Lauffenburger et al., 1983; Tranquillo et al., 1988). The configuration of the assay is illustrated in Fig. 4. The tissue culture dish is filled with Agarose (gel) and two wells are cut into the gel. One is filled with cells and the other is filled with a chemoattractant. The cells were described to have migrated towards the chemoattractant-containing well by squeezing under the gel. Fig. 5 shows the results obtained from the laboratory experiment (Hoffman et al., 1982).

To mimic the Under-Agarose Assay, we construct a virtual environment, shown in Fig. 6(a). The virtual environment is a 3 mm × 2 mm enclosed 2-D space. The space granularity ΔL (the distance between neighboring grid points) is set at 20 μm. The cell and attractant wells are both 250 μm in radius and are placed 1 mm apart. Initially, the cell well is filled with 1000 cells, and the attractant well is filled with attractant molecules at a concentration of 2500 particles per 20 μm × 20 μm area (for a total of about 1.2×10^6 molecules). By assuming a well height of 50 μm, we create a cell concentration of 10^3 cells μL^{-1} and a molecular concentration of 10^{-10} mol L^{-1} so as to be comparable to the original experiment setting (Heit and Kubes, 2003). The upper panel in Fig. 6 shows the 2-D positioning of the wells, and the lower panel shows the M cell histogram along the x-axis and the cross-sectional view (at central y position, $y = 1000$) of the attractant distribution. The cell radius is 4 μm and the maximum random speed is 2 μm min^{-1}. The molecules diffuse with diffusion constant $D = 10\,\mu m^2\,min^{-1}$. Table 4 summarizes the model parameters mentioned above and for the various chemotactic movement rules.

The real-time visualization of the simulation enables us to monitor any transient pattern emerges in the course of simulation. Fig. 6 shows a sample of the plot. The three panels are aligned by their x coordinates. Panel (a) is the top view of the cell distribution (cells as black dots) and molecule distribution (green corresponds to high concentration and white corresponds to low concentration). It is cropped to appropriate size to save the display space without loss of information. Panel (b) displays the agents (cells) distribution in the form of a histogram, with a bin width of ΔL. The height of each bin corresponds to the number of cells whose x coordinates happen to fall in the range that bin represents. Panel (b) also displays the sectional view of the molecular concentration distribution (in green) with the sectional plane indicated in panel (a). Panel (b) is *absolute in height* that the figure is *not* downscaled when the concentration drops or the cell count decreases. This facilitates the comparison of simulation patterns at different time instances. Panel (c) displays the x

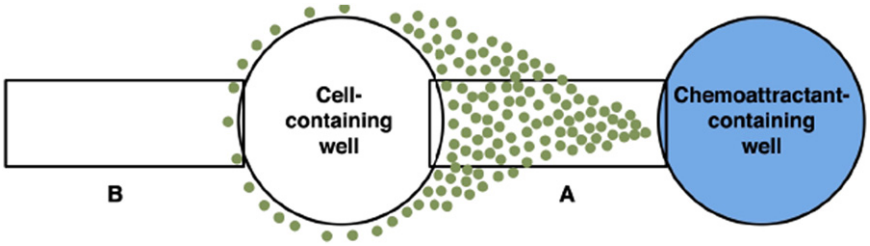

Fig. 4. Illustration of the Under-Agarose Assay (figure adopted from Heit and Kubes, 2003).

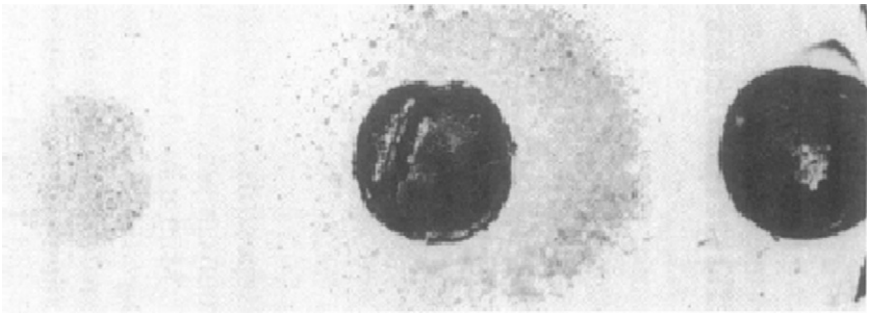

Fig. 5. Sample results of the Under-Agarose Assay (figure adopted from Hoffman et al., 1982).

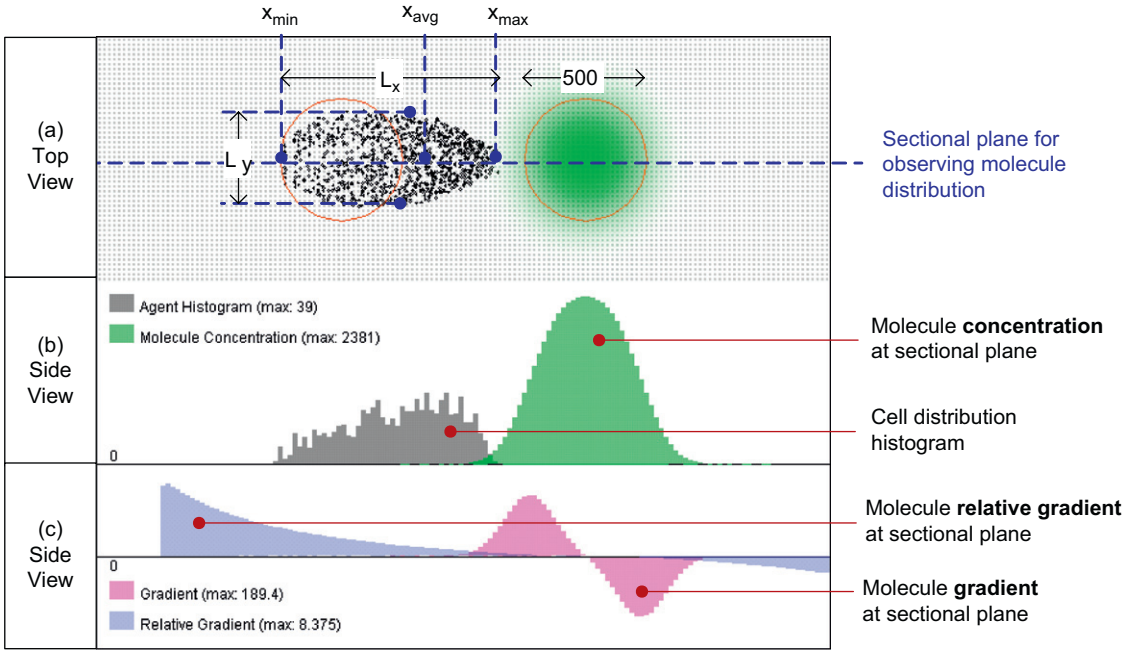

Fig. 6. Visualization of simulation result.

Table 4
Model parameters for simulating chemotaxis

Parameter	Value	Description
Δt	1 min	Update interval of molecular diffusions
ΔL	20 μm	Granularity of the site grid
D	10 μm^2 min	Diffusion constant of molecule L
λ	0 min^{-1}	Decay constant of molecule L (no spontaneous loss of molecules)
V	50 μm^2	Volume of M cell
r	4 μm	Radius of M cell
l	2 μm min	Random motility of M cell: max movement speed
R_{tot}	50,000	The total amount of receptor molecules R per M cell
K_r	0.5 min^{-1}	The recycle rate of internalized receptor R^*
K_b	2×10^{-6} min^{-1}	The association rate of L and R
K_i	0.3 min^{-1}	The internalization rate of occupied receptor LR

component of the molecular gradient at the sectional plane (i.e., the first partial derivative of concentration over x direction, *positive* means gradient pointing to the right) and the relative gradient (i.e., gradient divided by concentration, *positive* means relative gradient pointing to the right). Panel (c) display is *relative in height* that the figures are always re-scaled as the values change, so that the displayed heights of the maximal gradient and maximal relative gradient are fixed. The maximum values are displayed in the legend.

To quantify the comparisons of cell migration patterns, we measure the parameters shown in Fig. 6(a). The x coordinates of the front and the rear of the M cell population are denoted by x_{max} and x_{min}, respectively, and the mean x-coordinate of the entire cell population (i.e. center of mass) by x_{avg}. The initial values of x_{avg}, x_{max}, and x_{min} are 1000, 1250, and 750, respectively. L_x and L_y are the extensions of the pattern in the x and y directions. We use their ratio L_x/L_y as an estimate of the elongation of the migration pattern. Pattern elongation is caused by the speed difference between cells at the front and at the rear of the population. When the cell pattern is circular, L_x/L_y is 1. The larger the value of L_x/L_y, the more elongated the pattern.

The simulation model is implemented in Java. The simulation is run on a Windows XP Professional system with 2.4 GHz Pentium 4 CPU and 1 GB of Memory. One single run of the simulation of 5000 time steps takes approximately half a minute with the visualization refreshed at the interval 100 time steps.

4.3. Analysis of experimental results

As defined in Eq. (23), k is the proportional parameter that relates a cell's chemotactic displacement with the difference in newly bound receptors between this cell's front and rear. Therefore, the larger the k, the larger the chemotactic displacement is to be expected. Fig. 7 shows the simulation results at $t = 5000$ for k at 3, 10, 25, and 50.

Table 5 shows the measurable parameters for each k setting. The model produces a biased random walk pattern which is qualitatively close to the laboratory observation (Fig. 5) for low k values. Besides, following observations are made:

(1) As expected, the larger the k, the greater the displacement of the cells towards the chemoattractant. However, it can be seen from Fig. 7 that the cell population spreading towards right is sparsely distributed. The majority of the cell population is still concentrated in the cell well. This is further confirmed by values in Table 5. The cell population front x_{max} significantly increases with the increase of k, but the population center x_{avg} only slightly increases on a much smaller scale than x_{max}.
(2) The pattern elongation along the y-axis is evident from both the figures and the measurement of the parameters (i.e., $L_x/L_y > 1$) in Table 5.
(3) As for the cell population rear x_{min}, it decreases as k increases, that is, the cell population rear moves towards left.
(4) The molecule distribution exhibits a horseshoe shape, and its shape coincides spatially with the edge of the cell population. The area occupied by cells is low in attractant concentration, reflected by their lighter background.

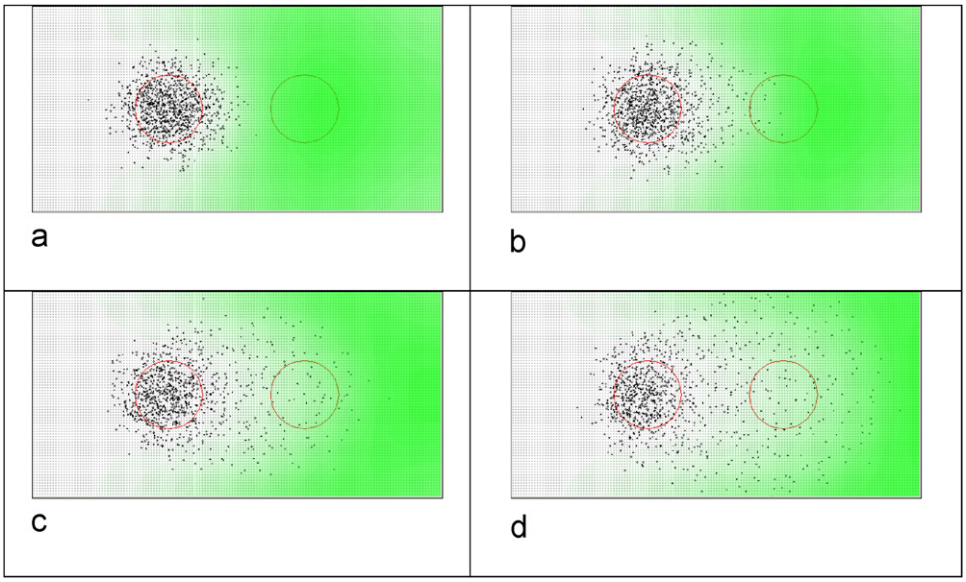

Fig. 7. Simulation results at $t = 5000$ with different k values: (a) $k = 3$, (b) $k = 10$, (c) $k = 25$ and (d) $k = 50$.

Table 5
Cell migration parameters at $t = 5000$

k	x_{avg}	x_{min}	x_{max}	L_x/L_y
3	1018.98	409.29	1644.49	1.275
10	1055.59	525.61	1990.38	1.375
25	1130.81	553.06	2622.43	1.604
50	1235.53	482.27	2858.61	1.380

The above observation can be attributed to the interactions between cells and attractant. As defined by the agent movement rules, the receptor–ligand binding leads to internalization of the ligand (attractant), effectively reducing the local concentration of the attractant. The cell population thus falls in a "basin" of the attractants concentration created by the cells themselves. The cells spread towards left due to *chemotactic* movement (as opposed to *random* movement), as the gradient at the population rear is pointing to the left.

Fig. 8 shows the measurable parameters for $k = 10$ and 25 for between the time $t = 0$ and $t = 5000$. The plots show the consistent increase of x_{max} (population front) and the consistent decrease of x_{min} (population rear). The pattern elongation L_x/L_y gradually increases then decreases, implying that the spread along y-axis become relatively more significant at the later stage of the simulation.

To further investigate the correlation between the cell population distribution, attractant concentration and gradient, we plot the snapshots of the simulation for $k = 25$ at $t = 1000$ and 5000, and compare them against the scenario where no cells exist in the environment, as shown in Fig. 9. One could immediately see the distinction in the smoothness of the gradient and relative gradient between the two scenarios. When there are no cells, the molecular distributions and the landscape of the gradient and relative gradient are smooth. This is expected as in this case, the molecular distribution is only affected by the diffusion equations and no other factors, since the cells are not present. However, when the cells are present, the landscape of the gradient and relative gradient become rugged, reflecting the local interactions between cells and molecules (that is, the cell receptors bind and "consume" the molecules in the local space).

At $t = 1000$, the front of the cell population towards the chemoattractant is evident, which spatially coincides with the peak of the gradient. The negative relative gradient starts to appear at the population rear, indicating that the gradient at that point is pointing towards left, that is, the cells at the population rear will be attracted towards left instead of right. This is in contrast with the scenario when cells are absent, where the gradient is always positive on the left to the attractant well (i.e., the gradient is pointing towards right). For $t = 5000$, almost half of the cell population falls in the area of negative gradients (which implies that cells at the rear are moving towards left) and the other half fall in the positive gradient (i.e., cells at the front are moving towards right). When compared to the scenario where the cells are absent, it can be seen that the gradient landscape is totally different, and the molecular concentrations are much lower. This further confirms that the basin-like distribution of molecular concentrations is indeed caused by the cells themselves through interactions (i.e., molecule consumptions) with the environment.

We further study the long-term simulation results by extending the simulation to $t = 20{,}000$ and 100,000. The results are shown in Fig. 10. It can be seen from the cell distribution (upper panel) as well as the cell histogram (mid-panel) that the cells are further spread over the space. The attractant concentration becomes so low that their effects on the cells are almost negligible. In the long run, cell movements become independent of attractants and collectively, exhibit a normal diffusion pattern.

The efficacy of the hybrid approach for designing agent-based models for microbiological systems has been demonstrated with an *in silico* simulation of the Under-Agarose assay for showing chemotaxis. The laboratory experiment for the Under-Agarose assay typically take at least 2–4 h for neutrophils (not counting the time for preparing materials and solutions), and can take as long as 18 h for slower cells such as monocytes (Heit and Kubes, 2003). The computer simulation has the obvious advantage that it completes much faster (in minutes in our example). As we are able to view the real-time cell migration pattern with a computer simulation, it is not so convenient to do the same in laboratory experiment. Observing the cell pattern usually requires staining the cells at the end of the experiment for them to be visible under microscope (Heit and Kubes, 2003), which means that only limited snapshots of the cell patterns can be obtained.

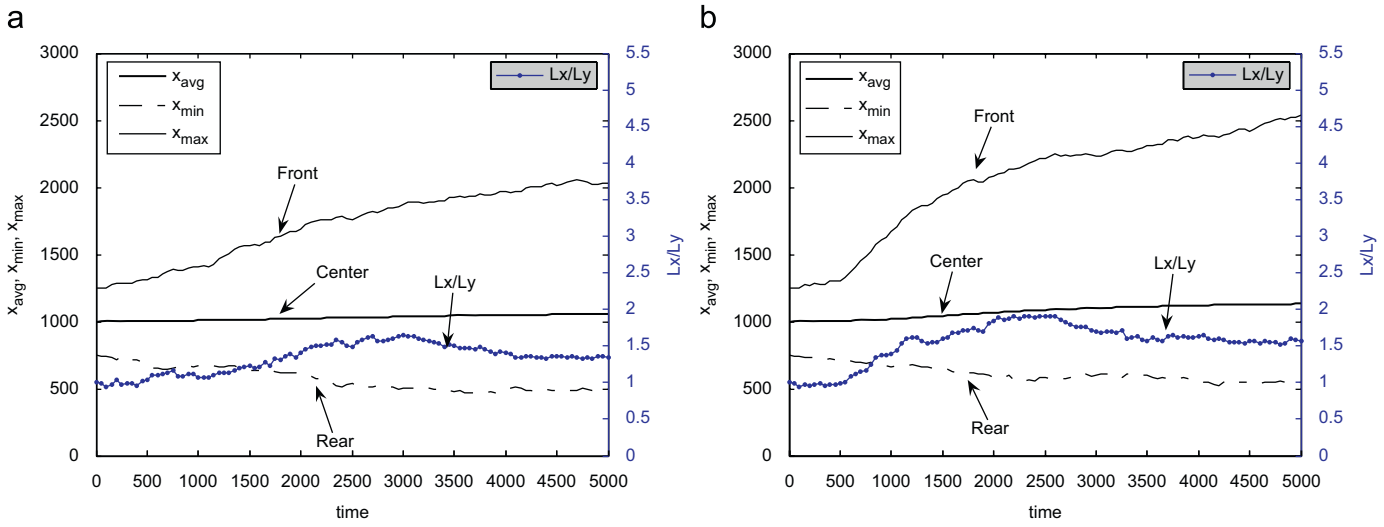

Fig. 8. Cell migration parameters: (a) $k = 10$ and (b) $k = 25$.

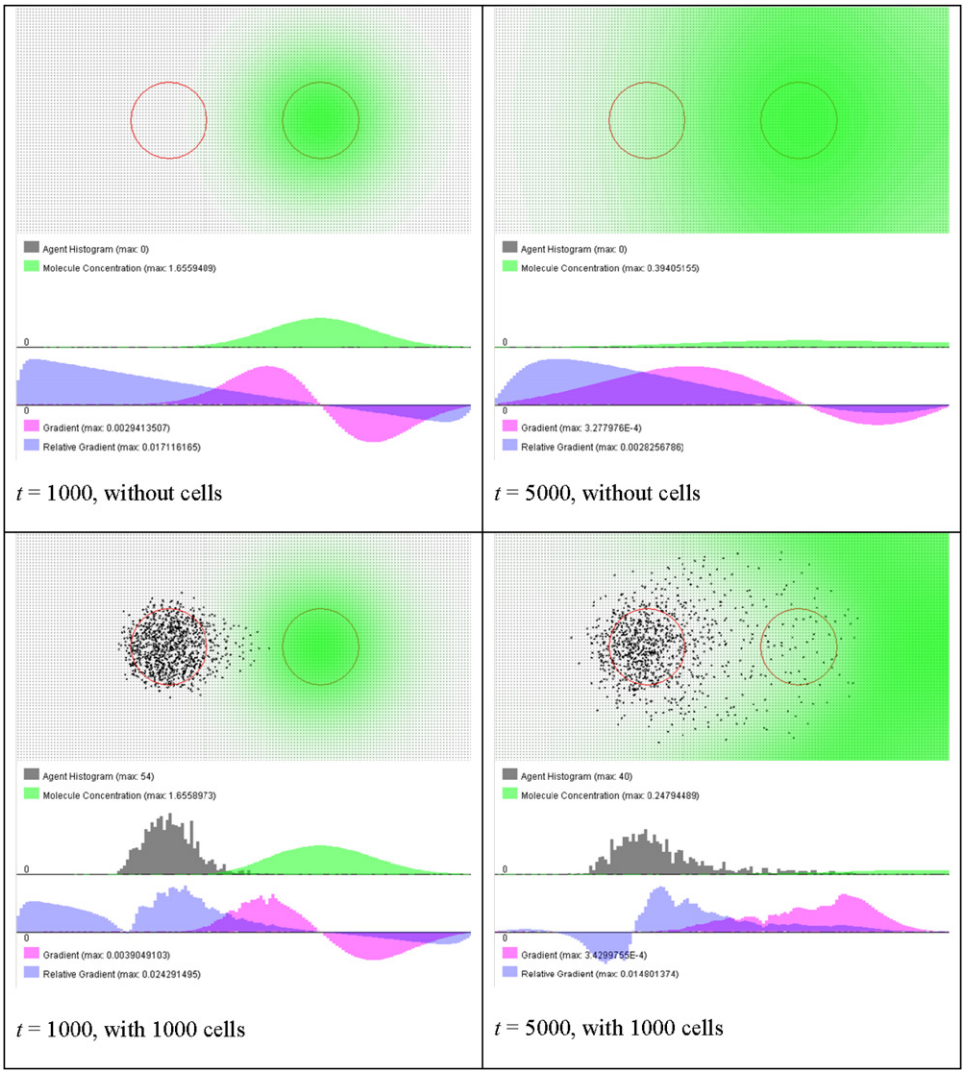

Fig. 9. Snapshots of the cell migration pattern, cell histogram, attractant concentration and gradient at $t = 1000$ and 5000 with $k = 25$.

Though our model produces the cell migration pattern that resembles the biased random work pattern, the similarity is mainly qualitative. For example, our model predicts that in the long term, cells eventually spread like random diffusions. But we do not yet know how long the laboratory experiment has to be in order for this to be verifiable, as we have not established a formal

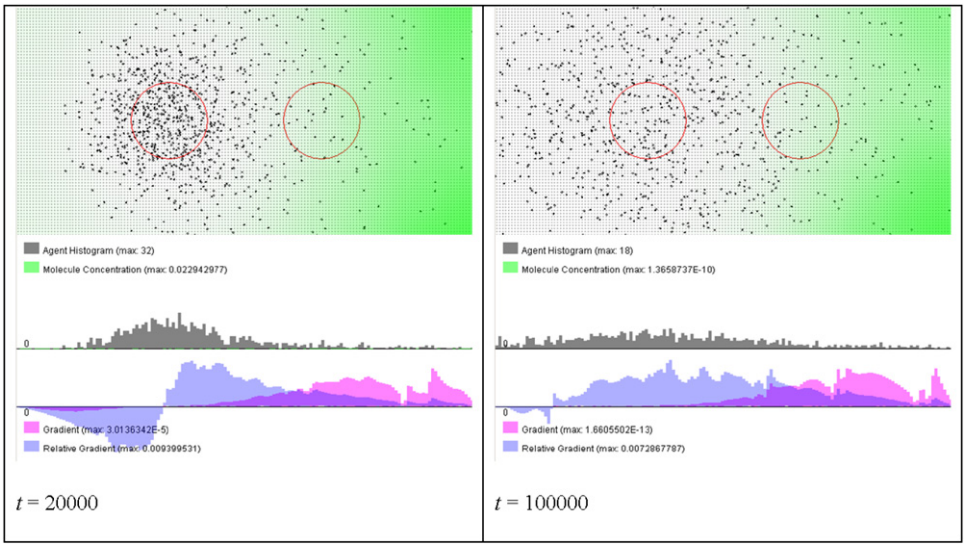

Fig. 10. Long-term results at $t = 20{,}000$ and 100,000 with $k = 25$.

correspondence between the time in the real world and the time in the simulation.

Our present model omits much of the intracellular mechanisms, but with the hybrid modeling approach, improvements on both the environment level (such as compartmentalized environment in the *in vivo* system) and individual level (such as adding intracellular signaling pathway that converts receptor–ligand binding into cell locomotions), can be made as and when granularity is justified by the hypothesis in question.

5. Conclusions

In the field of systems biology, system models are constructed with the objective of integrating the knowledge of cellular and molecular mechanisms for prediction of system dynamics as a whole. In applications to verify HIV pathogenesis hypotheses (the clinical patterns) against drug effects on immunological responses, it is necessary to increase the model granularity to include intracellular level molecular interactions, but at the same time keeping the model computationally tractable. Two commonly used modeling approaches, namely the Differential Equation approach and Multi-Agent approach, have generally been considered distinctive and mutually exclusive, but we have shown how both methods can be combined to achieve a balance in model granularity, computational tractability, and performance. In our hybrid agent-based modeling approach, biological cells are modeled as individual agents and molecules as quantities. The hybridization of the quantity-based macroscopic modeling (for molecules) and the individual-based microscopic modeling (for cells) exists at both the environment and individual levels. This is achieved by stratifying the environment into a continuous space layer (the Agent Holder Layer) and two discrete space layers (a Molecule Space Layer and a Flow Field Layer), where agents interact with the environment (e.g., molecular concentrations, gradients, flow directions) based on spatial proximity. At the individual level, our model allows a mixed representation of agent's state variables, from less-accurate discrete symbolic values (such as the healthy state) to more-accurate real values (such as receptor levels) through different types of update logics (or rules), ranging from simple value assignment (for symbolic values) to sophisticated coupled differential equations (for real values). Such a hybrid agent model allows for mixed and extendible levels of model granularity to cater to problem requirements. We demonstrate the efficacy of this approach with models of chemotaxis (directed cell movement), a phenomenon underlying many important biological functions. The model simulates an Under-Agarose assay of 10^3 cells and 1.2×10^6 molecules. The model successfully produces cell migration patterns that are qualitatively comparable to the laboratory observations. We have elaborated on the extendibility of this modeling approach in Guo and Tay (2008) with three models of chemotaxis with increasing model granularity.

References

Ander, M., Beltrao, P., Di Ventura, B., Ferkinghoff-Borg, J., Foglierini, M., Kaplan, A., Lemerle, C., Tomas-Oliveira, I., Serrano, L., 2004. SmartCell, a framework to simulate cellular processes that combines stochastic approximation with diffusion and localisation: analysis of simple networks. IEE Syst. Biol. 1 (1), 129–138.

Celada, F., Seiden, P.E., 1992. A computer model of cellular interactions in the immune system. Immunol. Today 13 (2), 56–62.

Cyster, J.G., 1999. Chemokines and the homing of dendritic cells to the T cell areas of lymphoid organs. J. Exp. Med. 189 (3), 447–450.

Cyster, J.G., 2000. Leukocyte migration: scent of the T zone. Curr. Biol. 10 (1), R30–R33.

Devreotes, P.N., Zigmond, S.H., 1988. Chemotaxis in eukaryotic cells: a focus on leukocytes and dictyostelium. Ann. Rev. Cell Biol. 4, 649–686.

Eisenbach, M., Lengeler, J.W., Varon, M., Gutnick, D., Meili, R., Firtel, R.A., Segall, J.E., Omann, G.M., Tamada, A., Murakami, F., 2004. Chemotaxis. Imperial College Press, London.

Emonet, T., Macal, C.M., North, M.J., Wickersham, C.E., Cluzel, P., 2005. AgentCell: a digital single-cell assay for bacterial chemotaxis. Bioinformatics 21 (11), 2714–2721.

Fauci, A.S., 2003. HIV and AIDS: 20 years of science. Nat. Med. 9 (7), 839–843.

Firtel, R.A., Chung, C.Y., 2000. The molecular genetics of chemotaxis: sensing and responding to chemoattractant gradients. BioEssays 22 (7), 603–615 doi:10.1002/1521-1878(200007)22:7<603::AID-BIES3>3.0.CO;2-#.

Grilo, A., Caetano, A., Rosa, A., 1999. Immune system simulation through a complex adaptive system model. In: Proceeding of the Third Workshop on Genetic Algorithms and Artificial Life.

Gross, D., Strand, R., 2000. Can agent-based models assist decisions on large-scale practical problems? A philosophical analysis. Complexity 5 (6), 26–33 doi:10.1002/1099-0526(200007/08)5:6<26::AID-CPLX6>3.0.CO;2-G.

Guo, Z., Tay, J.C., 2005. A comparative study of modeling strategies of immune system dynamics under HIV-1 infection. In: Lecture Notes in Computer Science, Banff, Albeta, Canada, vol. 3627, pp. 220–233.

Guo, Z., Tay, J.C., 2007. Multi-timescale event scheduling in multi-agent immune simulation models. Biosystems.

Guo, Z., Tay, J.C., 2008. Granularity and the validation of agent-based models. In: Proceedings of Agent-Directed Simulation Symposium (ADS'08), Ottawa, Canada.

Guo, Z., Han, H.K., Tay, J.C., 2005. Sufficiency verification of HIV-1 pathogenesis based on multi-agent simulation. In: Proceedings of the Genetic and Evolutionary Conference 2005, Washington, DC, vol. I, pp. 305–312.

Guyton, A.C., Hall, J.E., 2000. Textbook of Medical Physiology, 10th ed. Saunders, Philadelphia.
Heath, M.T., 2005. Scientific Computing: An Introductory Survey. McGraw-Hill, New York.
Heit, B., Kubes, P., 2003. Measuring chemotaxis and chemokinesis: the under-agarose cell migration assay. Sci. STKE 170, pl5.
Hoffman, R.D., Klingerman, M., Sundt, T.M., Anderson, N.D., Shin, H.S., 1982. Stereospecific chemoattraction of lymphoblastic cells by gradients of lysophosphatidylcholine. Proc. Natl. Acad. Sci. USA 79, 3285–3289.
Hosseini, P.R., 2006. Pattern formation and individual-based models: the importance of understanding individual-based movement. Ecol. Model. 194, 357–371.
Jacob, C., Litorco, J., Lee, L., 2004. Immunity through swarms: agent-based simulations of the human immune system. In: Proceedings of Third International Conference on Artificial Immune Systems, Catania, Sicily, Italy, vol. 3239, pp. 400–412.
Janeway, C.A., Travers, P., Walport, M., Shlomchik, M., 2001. Immunobiology: The Immune System in Health & Disease. Garland Science Publishing.
Jones, G.E., 2000. Cellular signaling in macrophage migration and chemotaxis. J. Leukoc. Biol. 68, 593–602.
Keller, E.F., Segel, L.A., 1971a. Model for chemotaxis. J. Theor. Biol. 30 (2), 225–234.
Keller, E.F., Segel, L.A., 1971b. Traveling bands of chemotactic bacteria: a theoretical analysis. J. Theor. Biol. 30 (2), 235–248.
Kitano, H., 2002. System biology: a brief overview. Science 295 (5560), 1662–1664.
Klabunde, R.E., 2006. Cardiovascular Physiology Concepts from 〈http://www.cvphysiology.com/Hemodynamics/H006.htm〉.
Kleinstein, S.H., Seiden, P.E., 2000. Simuating the immune system. Comput. Sci. Eng. 2 (4), 69–77.
Lauffenburger, D.A., Rothman, C., Zigmond, S.H., 1983. Measurement of leukocyte motility and chemotaxis parameters with a linear Under-Agarose Migration Assay. J. Immunol. 131 (2), 940–947.
Lin, F., Nguyen, C.M.-C., Wang, S.-J., Saadi, W., Gross, S.P., Jeon, N.L., 2004. Effective neutrophil chemotaxis is strongly influenced by mean IL-8 concentration. Biochem. Biophys. Res. Commun. 319 (2), 576–581.
Mathews, C.K., van Holde, K.E., Ahern, K.G., 2000. Biochemistry, third ed. Addison-Wesley, Longman, Reading, MA, NewYork.
Merieb, E.N., 2006. Essentials of Human Anatomy and Physiology, eighth ed. Pearson.
Mitchison, T.J., Cramer, L.P., 1996. Actin-based cell motility and cell locomotion. Cell 84 (3), 371–379.
Nelson, P., 2004. Biological Physics: Energy, Information, Life. W.H. Freeman and Company, New York.
Nowak, M.A., Anderson, R.M., McLean, A.R., Wolfs, T.F.W., Goudsmit, J., May, R.M., 1991. Antigenic diversity thresholds and the development of AIDS. Science 254 (5034), 963–969.
Parent, C.A., Devreotes, P.N., 1999. A Cell's sense of direction. Science 284 (5415), 765–770.
Perelson, A.S., Nelson, P.W., 1999. Mathematical analysis of HIV-1 dynamics in vivo. SIAM Rev. 41 (1), 3–44.
Railsback, S.F., Harvey, B.C., 2002. Analysis of habitat-selection rules using an individual-based model. Ecology 83 (7), 1817–1830 doi:10.1890/0012-9658(2002)083[1817:AOHSRU]2.0.CO;2.
Railsback, S.F., Hamberson, R.H., Harvey, B.C., Duffy, W.E., 1999. Movement rules for individual-based models of stream fish. Ecol. Model. 123 (2–3), 73–89.
Roitt, I.M., Delves, P.J., 2001. Essential Immunology, 10th ed. Blackwell Science, Oxford.
Sallusto, F., Schaerli, P., Loetscher, P., Schaniel, C., Lenig, D., Mackay, C.R., Shixin, Q., Lanzavecchia, A., 1998. Rapid and coordinated switch in chemokine receptor expression during dendritic cell maturation. Eur. J. Immunol. 28 (9), 2760–2769 doi:10.1002/(SICI)1521-4141(199809)28:09<2760::AID-IMMU2760>3.0.CO;2-N.
Sanchez-Madrid, F., Del Pozo, M.A., 1999. Leukocyte polarization in cell migration and immune interactions. EMBO J. 18 (3), 501–511.
Schaff, J., Fink, C.C., Slepchenko, B., Carson, J.H., Loew, L.M., 1997. A general computational framework for modeling cellular structure and function. Biophys. J. 73 (3), 1135–1146.
Sherratt, J.A., 1994. Chemotaxis and chemokinesis in eukaryotic cells: the Keller-Segel equations as an approximation to a detailed model. Bull. Math. Biol. 56 (1), 129–146.
Sloot, P.M.A., Tirado-Ramos, A., Altinatas, K., Bubak, M., Boucher, C., 2006. From molecule to man: decision support in individualized e-health. Computer 39 (11), 40–46.
Sozzani, S., Allavena, P., D'Amico, G., Imai, T., Yoshie, O., Bonecchi, R., Mantovani, A., 1998. Cutting edge: differential regulation of chemokine receptors during dendritic cell maturation: a model for their trafficking properties. J. Immunol. 161, 1083–1086.
Stekel, D.J., Parker, C.E., Nowak, M.A., 1997. A model of lymphocyte recirculation. Immunol. Today 18 (5), 216–221.
Stix, G., 2006. A new assault on HIV. Sci. Am. (June), 76–79.
Takahashi, K., Yugi, K., Hashimoto, K., Yamada, Y., Pickett, C.J.F., Tomita, M., 2002. Computational challenges in cell simulation: a software engineering approach. IEEE Intell. Syst. 17 (5), 64–71.
Takahashi, K., Arjunan, S.N.V., Tomita, M., 2005. Space in systems biology of signaling pathways-towards intracellular molecular crowding in silico. FEBS Lett. 579 (8), 1783–1788.
Tranquillo, R.T., Zigmond, S.H., Lauffenburger, D.A., 1988. Measurement of the chemotaxis coefficient for human neutrophils in the under-agarose migration assay. Cell Motil. Cytoskeleton 11, 1–15.
Wei, S.H., Parker, I., Miller, M.J., Cahalan, M.D., 2003. A stochastic view of lymphocyte motility and trafficking within the lymph node. Immunol. Rev. 195, 136–159.
Weninger, W., Crowley, M.A., Manjunath, N., von Andrian, U.H., 2001. Migratory properties of naive, effector, and memory CD8+ T cells. J. Exp. Med. 194 (7), 953–966.
Weyns, D., Omicini, A., Odell, J., 2006. Environment as a first class abstract in multiagent systems. Auton. Agents Multi-Agent Syst. 14, 5–30.
Zigmond, S.H., Sullivan, J.L., Lauffenburger, D.A., 1982. Kinetic analysis of chemotactic peptide receptor modulation. J. Cell Biol. 92, 34–43.